bioRxiv preprint doi: https://doi.org/10.1101/2020.10.08.331025; this version posted October 9, 2020. The copyright holder for this preprint (which was not certified by peer review) is the author/funder, who has granted bioRxiv a license to display the preprint in perpetuity. It is made available under aCC-BY 4.0 International license.

Title

Dementia risk factors modify hubs but leave other connectivity measures unchanged in asymptomatic individuals: a graph theoretical analysis.

Authors

Hannah Clarke, clarkehj@cardiff.ac.uk

- Cardiff University Brain Research Imaging Centre (CUBRIC), School of Psychology, Cardiff University, Cardiff, CF24 4HQ, UK
- School of Medicine, UK Dementia Research Institute, Cardiff University, Cardiff, UK

Eirini Messaritaki, MessaritakiE2@cardiff.ac.uk

- Cardiff University Brain Research Imaging Centre (CUBRIC), School of Psychology, Cardiff University, Cardiff, CF24 4HQ, UK
- BRAIN Biomedical Research Unit, School of Medicine, Cardiff University, Maindy Road, Cardiff, CF24 4HQ, UK

Stavros I Dimitriadis, dimitriadiss@cardiff.ac.uk / stidimitriadis@gmail.com

- Cardiff University Brain Research Imaging Centre (CUBRIC), School of Psychology, Cardiff University, Cardiff, CF24 4HQ, UK
- Neuroinformatics Group, Cardiff University Brain Research Imaging Centre, School of Psychology, Cardiff University, Cardiff, UK
- Division of Psychological Medicine and Clinical Neurosciences, School of Medicine, Cardiff University, Cardiff, UK
- School of Psychology, Cardiff University, Cardiff, UK
- Neuroscience and Mental Health Research Institute, School of Medicine, Cardiff University, Cardiff, UK
- MRC Centre for Neuropsychiatric Genetics and Genomics, School of Medicine, Cardiff University, Cardiff, UK

Claudia Metzler-Baddeley, metzler-baddeleyc@cardiff.ac.uk

bioRxiv preprint doi: https://doi.org/10.1101/2020.10.08.331025; this version posted October 9, 2020. The copyright holder for this preprint (which was not certified by peer review) is the author/funder, who has granted bioRxiv a license to display the preprint in perpetuity. It is made available under aCC-BY 4.0 International license.

- Cardiff University Brain Research Imaging Centre (CUBRIC), Maindy Road, Cathays, Cardiff, CF24 4HQ, UK
- Neuroscience and Mental Health Research Institute, School of Medicine, Cardiff University, Cardiff, UK

Corresponding Author

Claudia Metzler-Baddeley, metzler-baddeleyc@cardiff.ac.uk, Cardiff University Brain Research Imaging Centre (CUBRIC), Maindy Road, Cathays, Cardiff, CF24 4HQ, UK

Authorship confirmation statement

- HC ran the analysis and drafted the methods and results sections.
- EM provided MATLAB code for the analysis, contributed to study design, and drafted parts of the manuscript.
- SID provided MATLAB code for the analysis, contributed to study design and drafted the manuscript.
- CMB was responsible for the conceptualization of CARDS, draft review & editing, and funding acquisition.

All authors approved the final version of the manuscript.

Key Words

- Alzheimer's Disease
- Graph Theoretical Analysis
- Risk factors
- Hubs

bioRxiv preprint doi: https://doi.org/10.1101/2020.10.08.331025; this version posted October 9, 2020. The copyright holder for this preprint (which was not certified by peer review) is the author/funder, who has granted bioRxiv a license to display the preprint in perpetuity. It is made available under aCC-BY 4.0 International license.

Abstract

Background: Alzheimer's Disease (AD) is the most common form of dementia with genetic and environmental risk contributing to its development. Graph theoretical analyses of brain networks constructed from structural and functional MRI measurements have identified connectivity changes in AD and individuals with mild cognitive impairment (MCI). However, brain connectivity in asymptomatic individuals at risk of AD remains poorly understood.

Methods: We acquired diffusion-weighted magnetic resonance imaging (dMRI) data from 165 asymptomatic individuals (38-71 years) from the Cardiff Ageing and Risk of Dementia Study (CARDS). We calculated white matter tracts and constructed whole-brain, default-mode-network and visual structural brain networks that incorporate multiple structural metrics as edge weights. We then calculated the relationship of three AD risk factors, namely Apolipoprotein-E ε4 genotype (APOE4), family history (FH) of dementia, and central obesity, on graph theoretical measures and hubs**.**

Results: We observed no risk-related differences in clustering coefficients, characteristic path lengths, eccentricity, diameter and radius across the whole-brain, default-mode-network or visual system. However, a hub in the right paracentral lobule was present in all high-risk groups (FH, APOE4, obese) but absent in low-risk groups (no FH, APOE4-ve, healthy weight).

Discussion: We identified no risk-related effects on graph theoretical metrics in the structural brain networks of cognitively healthy individuals. However, high-risk was associated with a hub in the right paracentral lobule, an area with motor and sensory functions related to the lower limb. If this phenotype is shown to predict symptom development in longitudinal studies, it could be used as an early biomarker of AD.

Impact Statement

Alzheimer's Disease is a common form of dementia which to date has no cure. Identifying early biomarkers will aid the discovery and development of treatments that may slow AD progression in the future. In this paper we report that asymptomatic individuals at heightened

bioRxiv preprint doi: https://doi.org/10.1101/2020.10.08.331025; this version posted October 9, 2020. The copyright holder for this preprint (which was not certified by peer review) is the author/funder, who has granted bioRxiv a license to display the preprint in perpetuity. It is made available under aCC-BY 4.0 International license.

risk of dementia due to their family history, Apolipoprotein-E ε4 genotype and body adiposity have a hub in the right paracentral lobule which is absent in low-risk groups. If this phenotype were to predict the development of symptoms in a longitudinal study of the same cohort, it could provide an early biomarker of disease progression.

Introduction

Alzheimer's disease (AD) is one of the major causes of dementia that affects 10% of individuals over the age of 65. In the United States, over one million individuals per year will be affected by AD by 2050 (Hebert et al., 2013). A recent review by the Lancet Commission concluded that almost half of dementia cases might be prevented or delayed by modifying 12 risk factors (Livingston et al., 2020). It emphasized the importance of improving the early detection of individuals at risk of developing AD so that preventative therapeutics can be discovered and developed in the future. It is therefore important to gain a better understanding of how AD risk factors affect the structure of the brain in healthy individuals and how risk-related effects differ from those of healthy aging.

The human brain has been characterized as a network of cortical and subcortical areas (network nodes) which communicate with each other via white matter tracts (connections, or edges) that carry neuronal signals (E. T. Bullmore & Bassett, 2011; Rubinov & Sporns, 2010). Structural networks can be derived from diffusion-weighted magnetic resonance imaging (dMRI) data via tractography (Basser et al., 2000; Mukherjee, Berman, et al., 2008; Mukherjee, Chung, et al., 2008), and are represented mathematically by graphs. Graph theory can then be employed to quantify the local and global organizational properties of the brain's structural connectome (E. Bullmore & Sporns, 2009). Graph theoretical analyses of brain networks have provided insight into the effect of AD on the brain's connectivity (Dai et al., 2019; John et al., 2017; Lo et al., 2010). More specifically, there is strong evidence that, even though AD pathology is initially present in localized brain areas, it still affects the whole brain as a network. It is, therefore, possible that people at risk of developing AD could show alterations in their structural brain networks and their graph theoretical metrics before developing the disease.

bioRxiv preprint doi: https://doi.org/10.1101/2020.10.08.331025; this version posted October 9, 2020. The copyright holder for this preprint (which was not certified by peer review) is the author/funder, who has granted bioRxiv a license to display the preprint in perpetuity. It is made available under aCC-BY 4.0 International license.

This implies that investigations into possible relationships between AD risk factors and graph theoretical metrics of structural brain networks could provide biomarkers that signal disease onset or track disease progression.

In the present study, we used graph theory to characterize the mesoscale of structural brain networks for the whole-brain connectome and for systems that are affected in AD, namely the default mode network (DMN), as well as the visual network as a control (Badhwar et al., 2017), in 165 cognitively healthy individuals from the Cardiff Ageing and Risk of Dementia Study (CARDS) (38-71 years) (Coad et al., 2020; Metzler-baddeley, Mole, Leonaviciute, et al., 2019; Metzler-baddeley, Mole, Sims, et al., 2019; Mole et al., 2020) with different risk factors for AD. The risk factors investigated were central obesity, family history of dementia (FH) and Apolipoprotein-E ε4 (APOE4). A statistical framework was followed to reveal potential differences in structural network organization between groups of aggregated risk levels. Our hypothesis was that individuals at the highest risk of dementia, i.e. obese APOE4 carriers with a family history of dementia, compared to those at lowest risk, i.e. normal-weighted non-carriers without a family history, would have altered integration and segregation parameters (increased characteristic path lengths, decreased clustering etc).

1. Materials and Methods

Details of the CARDS study have been previously published (Coad et al., 2020; Metzler-baddeley, Mole, Leonaviciute, et al., 2019; Metzler-baddeley, Mole, Sims, et al., 2019; Mole et al., 2020) and will hence only be briefly described in the following. The CARDS study was approved by the School of Psychology Research Ethics Committee at Cardiff University (EC.14.09.09.3843R2) and all participants provided written informed consent.

1.1 Participants

Middle-aged and older participants were recruited from the local community via Cardiff University community panels, notice boards and poster advertisements. Exclusion criteria included a history of neurological and/or psychiatric disease, severe head injury, drug or

bioRxiv preprint doi: https://doi.org/10.1101/2020.10.08.331025; this version posted October 9, 2020. The copyright holder for this preprint (which was not certified by peer review) is the author/funder, who has granted bioRxiv a license to display the preprint in perpetuity. It is made available under aCC-BY 4.0 International license.

alcohol dependency, high risk cardio-embolic source or known significant large-vessel disease. MRI screening criteria were fulfilled by 166 participants (38-71 years of age). Table 1 summarises their demographic background, and information about their genetic and lifestyle risk variables. Depression was screened for with the Patient Health Questionnaire (PHQ-9) (Kroenke et al., 2001), verbal intellectual function was assessed with the National Adult Reading Test (NART) (Nelson, 1991) and cognitive impairment with the Mini Mental State Exam (MMSE) (Folstein et al., 1975). One participant was excluded after assessment of their MMSE score.

1.2 Assessment of risk factors

Participants gave saliva samples with the Genotek Oragene-DNA kit (OG-500) for *APOE* genotyping. *APOE* genotypes ε2, ε3 and ε4 were determined by TaqMan genotyping of single nucleotide polymorphism (SNP) rs7412 and KASP genotyping of SNP rs429358 (Metzler-baddeley, Mole, Leonaviciute, et al., 2019). Genotyping was successful for 164 of the 165 participants. In addition, 163 participants provided information about their family history of dementia, i.e. whether a first-grade relative was affected by AD, vascular dementia or any other type of dementia. We also obtained the number of years spent in education for 164 participants, to include as a covariate in this analysis (Table 1).

Participants' waist and hip circumferences were measured to calculate the waist-hip-ratio (WHR). Central obesity was defined as a WHR ≥ 0.9 for men and ≥ 0.85 for women (Table 1). Other metabolic risk factors were self-reported in a medical history questionnaire (see for details Mole et al., 2020) but were not included in the present analysis.

1.3 MRI data acquisition

MRI data were collected on a 3T MAGNETOM Prisma clinical scanner (Siemens Healthcare, Erlangen, Germany) (Coad et al., 2020; Metzler-baddeley, Mole, Leonaviciute, et al., 2019; Metzler-baddeley, Mole, Sims, et al., 2019; Mole et al., 2020) at the Cardiff University Brain Research Imaging Centre (CUBRIC). A 3D magnetization-prepared rapid gradient-echo (MP-

bioRxiv preprint doi: https://doi.org/10.1101/2020.10.08.331025; this version posted October 9, 2020. The copyright holder for this preprint (which was not certified by peer review) is the author/funder, who has granted bioRxiv a license to display the preprint in perpetuity. It is made available under aCC-BY 4.0 International license.

RAGE) sequence was used to acquire T_1-weighted anatomical images with the following parameters: 256x256 acquisition matrix, TR = 2300 ms, TE = 3.06 ms, TI = 850 ms, flip angle θ = 9°, 176 slices, 1 mm slice thickness, 1x1x1 mm isotropic resolution, FOV = 256 mm and acquisition time of ~ 6 min.

Diffusion-weighted MR images were acquired with High Angular Resolution Diffusion Imaging (HARDI) (Tuch et al., 2002) using a spin-echo echo-planar dual shell HARDI sequence with diffusion encoded along 90 isotropically distributed orientations (Jones et al., 1999) (30 directions at b-value = 1200 s/mm^2, 60 directions at b-value = 2400 s/mm^2) as well as six non-diffusion weighted images with dynamic field correction using the following parameters: TR = 9400ms, TE = 67ms, 80 slices, 2 mm slice thickness, 2x2x2 mm voxel, FOV = 256x256x160 mm, GRAPPA acceleration factor = 2, acquisition time of ~15 min.

1.4 HARDI data processing and whole brain tractography

Diffusion-weighted imaging data processing has been previously detailed in Coad et al., 2020; Metzler-baddeley, Mole, Leonaviciute, et al., 2019; Metzler-baddeley, Mole, Sims, et al., 2019; Mole et al., 2020. In brief, dual-shell data were split and b = 1200 and 2400 s/mm^2 data were corrected separately for distortions induced by the diffusion-weighted gradients and motion artefacts in ExploreDTI (v4.8.3) (Leemans et al., 2009). EPI-induced geometrical distortions were corrected by registering the diffusion-weighted image volumes to the T_1-weighted images (Irfanoglu et al., 2012).

Outliers in the diffusion data were identified with the RESDORE algorithm (Parker, 2014). Whole brain tractography was performed with the damped Richardson-Lucy algorithm (dRL) (Dell'Acqua et al., 2010) on the 60 direction, b = 2400 s/mm^2 HARDI data for each dataset in single-subject space using in-house software (Parker, 2014) coded in MATLAB (the MathWorks, Natick, MA). Fibre tracts were reconstructed by estimating the dRL fibre orientation density functions (fODFs) at the centre of each image voxel with seed points positioned at the vertices of a 2x2x2 mm grid superimposed over the image. At each seed point the tracking algorithm interpolated local fODF estimates and then propagated 0.5 mm

bioRxiv preprint doi: https://doi.org/10.1101/2020.10.08.331025; this version posted October 9, 2020. The copyright holder for this preprint (which was not certified by peer review) is the author/funder, who has granted bioRxiv a license to display the preprint in perpetuity. It is made available under aCC-BY 4.0 International license.

along orientations of each fODF lobe above a threshold of a peak amplitude of 0.05. Individual streamlines were then propagated by interpolating the fODF at their new location and by propagating 0.5 mm along the minimally subtending fODF peak. This process was repeated until the minimally subtending peak magnitude fell below 0.05 or the change of direction exceeded an angle of 45°. Tracking was subsequently repeated in the opposite direction from the initial seed point. Streamlines with lengths outside a range of 10 mm to 500 mm were removed.

1.5 Generating integrated weighted structural brain networks: whole-brain analysis

Whole brain tractography maps were used in ExploreDTI v4.8.6 (Leemans et al., 2009), to create connectivity matrices that describe the structural connectome mathematically. Network nodes were defined according to the automated anatomical labelling (AAL) atlas (Tzourio-Mazoyer et al., 2002), using the 90 cortical and subcortical areas of the cerebrum. The edges of the networks were the tractography-reconstructed tracts: all edges between brain areas not connected by tracts were therefore equal to zero. This process resulted in 16 90x90 connectivity matrices, the edges of each quantifying if there was a tract or not, number of tracts between two nodes, percentage of tracts between two nodes, average tract length, Euclidean distance, density of tracts, tract volume, mean diffusivity, axial diffusivity, radial diffusivity, fractional anisotropy, second and third eigenvalue of the diffusion tensor, linear anisotropy, planar anisotropy and spherical anisotropy.

The above-mentioned metrics are chosen because they could reflect the signal transport and integration abilities of the structural connectome. However, it is not clear yet to what extent they achieve that (Messaritaki et al., 2020). Additionally, the strength of the structural connectivity between brain areas depends on the metric used to weight the network edges. As a result, the network measures derived via the graph theoretical analysis depend on the connectivity matrix used – i.e. which of the above metrics we chose as an edge weight. We have recently shown that this ambiguity can be solved by linearly combining nine normalised metrics (number of tracts, percentage of tracts, average tract length, Euclidean

bioRxiv preprint doi: https://doi.org/10.1101/2020.10.08.331025; this version posted October 9, 2020. The copyright holder for this preprint (which was not certified by peer review) is the author/funder, who has granted bioRxiv a license to display the preprint in perpetuity. It is made available under aCC-BY 4.0 International license.

distance, density, tract volume, mean diffusivity, radial diffusivity and fractional anisotropy) into a single graph (Dimitriadis, Drakesmith, et al., 2017) and thresholding the subsequent graphs using an orthogonal minimal spanning trees scheme (Dimitriadis, Antonakakis, et al., 2017). This protocol creates connectivity matrices that combine the information from the included metrics in a data driven manner, so that the maximum information from all metrics is retained in the final graph; these are termed integrated graphs. The thresholding step can be applied in dense matrices, resulting in a topographically filtered integrated weighted structural brain networks. The network and nodal reliability of such integrated graphs was improved beyond that of the 9 individual metrics (Dimitriadis, Drakesmith, et al., 2017). In addition, they were shown to have very good discrimination capability in a binary classification problem (Dimitriadis, Drakesmith, et al., 2017), and to exhibit good scan-rescan reliability (Messaritaki et al., 2019). A recent study demonstrated that community partitions and provincial hubs are highly reproducible in a test-retest study when structural brain networks were constructed with the integrated approach (Dimitriadis et al., 2020). For those reasons we created integrated weighted brain networks instead of pursuing a single-metric structural connectivity matrix.

In order to reduce the number of false positives possibly resulting from the tractography, we set to zero all edges in the structural connectivity matrices that correspond to tracts with fewer than 5 streamlines (excluding Euclidean distance as this is a biological metric and has a value regardless of the number of streamlines). All subsequent analyses were performed on these thresholded connectivity matrices (Figure 1).

In order to decide which metrics to combine into the integrated weighted structural brain network, we calculated the intercorrelation coefficients (Corrcoef, MATLAB R2015a) between the number of tracts (NS), percentage of tracts (PS), average tract length (ATL), Euclidean distance (ED), density of streamlines (SLD), tract volume (TV), mean diffusivity (MD), radial diffusivity (RD), axial diffusivity (AxD) and fractional anisotropy (FA), see table 2. In addition, we performed a multicollinearity test (Collintest, MATLAB R2015a) in an endeavour to eliminate metrics representing redundant information within our integrated graphs. After excluding highly correlated and multi-collinear metrics, the remaining metrics

bioRxiv preprint doi: https://doi.org/10.1101/2020.10.08.331025; this version posted October 9, 2020. The copyright holder for this preprint (which was not certified by peer review) is the author/funder, who has granted bioRxiv a license to display the preprint in perpetuity. It is made available under aCC-BY 4.0 International license.

were integrated into a single graph via a linear graph-distance combination (Dimitriadis, Drakesmith, et al., 2017)[1].

1.6 Calculating network measures from integrated graphs

The resulting graphs were weighted and undirected. Using the MATLAB Brain Connectivity Toolbox (Rubinov & Sporns, 2010) we calculated the following metrics:

- Clustering coefficient: A measure of how interconnected nodes are (averaged across all nodes)
- Characteristic path length: The average minimum number of connections to span two nodes
- Eccentricity: Maximum shortest distance between one node and all others (averaged across all nodes)
- Radius: Minimum eccentricity
- Diameter: Maximum eccentricity
- Global efficiency: Inverse of the characteristic path length[2]

Network measures were examined for multicollinearity using Belsley collinearity diagnostics (Collintest, MATLAB R2015a) to ensure only unique predictors were included in our analysis. The remaining network measures were analysed using multivariate general linear models described below. We were also interested in identifying potential interactions between our risk factors.

1.6 Sub-network analysis

As AD preferentially impacts the DMN we repeated the analysis for this sub-network by adapting the AAL atlas (Tzourio-Mazoyer et al., 2002) based on the data from Power et al., 2011. The DMN graphs were comprised of 22 nodes from each hemisphere encompassing the frontal, temporal, parietal lobes including the precuneus, cingulate gyrus and hippocampus

[1] https://github.com/stdimitr/integrated_structural_brain_networks
[2] https://github.com/stdimitr/Network_Metrics

bioRxiv preprint doi: https://doi.org/10.1101/2020.10.08.331025; this version posted October 9, 2020. The copyright holder for this preprint (which was not certified by peer review) is the author/funder, who has granted bioRxiv a license to display the preprint in perpetuity. It is made available under aCC-BY 4.0 International license.

(Figure 2). To investigate if any changes were specific to the DMN we analysed a separate control sub-network – the visual system (Wang et al., 2012) by adjusting the regions of interest specified in Power et al., 2011. The resulting integrated weighted structural brain networks were composed of 16 nodes from the left and right hemispheres: inferior temporal gyrus, fusiform gyrus, superior/middle/inferior occipital gyrus, lingual gyrus, cuneus and calcarine fissure and surrounding cortex (Figure 2).

1.7 Hub analysis

Hubs are nodes of a network that are highly connected to other nodes and act as bridges that facilitate the transfer of signals in the brain, contributing to its integration abilities (van den Heuvel & Sporns, 2013). Crucially, hubs appear to play a role in AD (Buckner et al., 2009). We split the cohort into risk factor groups (positive vs. negative family history, APOE4 carriers vs. non-carriers, centrally obese vs. healthy weight) to explore whether hubs changed as a function of risk factor profile in healthy individuals. Hubs were identified across the whole-brain for each participant by ranking nodal betweenness centrality and strength, where higher scores indicate hubs. In addition, nodal local efficiency and clustering coefficients were ranked, with smaller values indicating hubs. A node was defined as a hub when it was in the top 20% for global measures and the lowest 20% for local measures. Using replicator dynamics (Dimitriadis et al., 2010; Neumann et al., 2005), hubs which were consistently present across the individual risk factor cohorts were determined[3].

1.8 Statistical analyses

Statistical analyses were performed in SPSS v26 (IBM Corp., 2019). We performed multivariate general linear models with factors of APOE4 carrier/non-carrier, family history of dementia/no family history and waist-hip ratio obese/healthy on dependent variables; mean clustering coefficient, characteristic path length, eccentricity, global efficiency, diameter and

[3] https://github.com/stdimitr/consistent_hubs_cohort

bioRxiv preprint doi: https://doi.org/10.1101/2020.10.08.331025; this version posted October 9, 2020. The copyright holder for this preprint (which was not certified by peer review) is the author/funder, who has granted bioRxiv a license to display the preprint in perpetuity. It is made available under aCC-BY 4.0 International license.

radius. The analyses were adjusted for covariates: age, years of education and sex. To ensure assumptions were met, normality of residuals was tested using Kolmogorov-Smirnov tests.

2. Results

2.1 Inclusion of metrics into integrated networks using correlation and collinearity tests

A multicollinearity test was performed on the 10 variables with a default cut-off of 30 for the condition index and 0.5 for proportion of variance-decomposition. This analysis revealed multicollinearity between AxD, MD and RD (Table 3). Correlation coefficients (Table 4) were calculated between all 10 connectivity metrics. We used a cut off of $R > 0.6$ to flag strong correlations to investigate further. PS, NS and TV were highly inter-correlated, and for that reason we only included NS in our analysis. AxD, MD and RD exhibit multicollinearity and both AxD and RD correlated strongly with FA ($R = 0.6036$, p-value $< 10^{-8}$ and $R = -0.6721$, p-value $< 10^{-8}$, respectively) – thus these two metrics were excluded. This resulted in a final inclusion of ATL, SLD, FA, ED, MD and NS. We re-ran the correlation and multicollinearity analysis on these metrics and confirmed no strong correlations (Table 4) or multicollinearity. These six metrics were then combined into a single graph (Figure 3) with an algorithm introduced in our previous study (Dimitriadis, Drakesmith, et al., 2017).

2.2. Exclusion of mean eccentricity from further analyses

Belsley collinearity diagnostics applied over the adopted set of network metrics flagged multicollinearity between diameter and mean eccentricity using whole-brain network measures (Table 5). We therefore excluded the eccentricity from further analyses and kept the diameter, which in combination to radius inform us about the lower (radius) and upper limits (diameter) of eccentricity.

2.3 Whole-brain analysis

Kolmogorov-Smirnov tests for normality revealed non-Gaussian distributions for all network measures (p-value < 0.05, Table 6, Figure S1). To alleviate this, diameter, characteristic path length and radius were log transformed to reduce positive skew, and efficiency and clustering

bioRxiv preprint doi: https://doi.org/10.1101/2020.10.08.331025; this version posted October 9, 2020. The copyright holder for this preprint (which was not certified by peer review) is the author/funder, who has granted bioRxiv a license to display the preprint in perpetuity. It is made available under aCC-BY 4.0 International license.

coefficients were squared to reduce negative skew. One extreme outlier was present in the diameter data after transformation (defined as > 3 x interquartile range) thus we excluded this participant from further whole-brain analyses. After data cleaning, the diameter, characteristic path length, and radius were normally distributed (p-value > 0.05), but efficiency and clustering coefficients were non-normal. Despite this the analysis was continued after visual examination of the distribution of residuals (Figure S1). Four participants were missing data thus the final analysis had a sample size of 160. Omnibus multivariate analyses revealed no significant main or interaction effects (p-value > 0.05, Table 7), suggesting that there were no differences in whole-brain network measures between individuals who carry APOE4 vs. non-carriers, have a FH vs. no FH, obese vs. healthy weight.

2.4 Sub-network analyses

We then investigated whether any individual differences were occurring at a sub-network level.

2.4.1 Default Mode Network analysis

Kolmogorov-Smirnov tests revealed non-normality for all network measures calculated from the DMN integrated graphs (Table 6, Figure S2). To correct for this, the diameter, characteristic path length and radius were log transformed and the efficiency was squared. Despite being non-Gaussian as determined by Kolmogorov-Smirnov tests, the distribution of residuals for mean clustering coefficients was not transformed after visual inspection. We identified nine extreme outliers (> 3 x interquartile range) within efficiency data and one within clustering coefficients thus these were removed from the analysis. After data cleaning, the characteristic path length, efficiency and clustering coefficients were not formally normal when reassessed with Kolmogorov-Smirnov tests, however the analysis was continued (Figure S2) with a sample size of 151. Multivariate analyses revealed no significant effects (p-value > 0.05, Table 7) suggesting that there are no differences in default mode network measures as a result of risk-factor profile.

2.4.2 Visual network analysis

bioRxiv preprint doi: https://doi.org/10.1101/2020.10.08.331025; this version posted October 9, 2020. The copyright holder for this preprint (which was not certified by peer review) is the author/funder, who has granted bioRxiv a license to display the preprint in perpetuity. It is made available under aCC-BY 4.0 International license.

Kolmogorov-Smirnov tests revealed non-normality for all six network measures for the visual system (Table 6, Figure S3). Following the same process as before, the diameter, characteristic path length and radius were log transformed and the efficiency and clustering coefficients were squared. No outliers were identified in the transformed metrics. Diameter, characteristic path length, radius and efficiency were non-normal, however the analysis was continued (Figure S3) with a sample size of 161. The general linear model revealed no significant multivariate effects (Table 7).

2.5 Analysis of network hubs in the whole-brain

Replicator dynamics identified hubs consistent across the individual risk factor groups. Individuals with no FH had hubs located in the left and right rolandic operculum, right inferior parietal gyrus, left angular gyrus and right Heschl's gyrus, whereas individuals with a positive FH had hubs at the right rolandic operculum, left inferior frontal gyrus opercular part, left and right paracentral lobule and the right Heschl's gyrus (Figure 4). Individuals who were of healthy weight, and thus considered at less risk of developing AD, had hubs within the left inferior frontal gyrus opercular part, right rolandic operculum, right inferior parietal gyrus and right Heschl's gyrus, whereas individuals who were obese had hubs within the right rolandic operculum, right paracentral lobule and both left and right Heschl's gyrus (Figure 4). Participants who were negative for the APOE4 allele (and thus considered low-risk), had hubs in the left inferior frontal gyrus opercular part, right rolandic operculum, right precuneus and right Heschl's gyrus whereas APOE4 positive individuals had hubs in the right rolandic operculum, right inferior parietal gyrus, left angular gyrus, right paracentral lobule and right Heschl's gyrus (Figure 4).

To summarise the above described pattern, the right rolandic operculum and Heschl's gyrus remain present as hubs regardless of risk factor. In contrast, at risk individuals (obese, positive FH and APOE4 carriers) consistently have a hub in the right paracentral lobule which is absent in their respective low-risk group (Table 8, Figure 4).

bioRxiv preprint doi: https://doi.org/10.1101/2020.10.08.331025; this version posted October 9, 2020. The copyright holder for this preprint (which was not certified by peer review) is the author/funder, who has granted bioRxiv a license to display the preprint in perpetuity. It is made available under aCC-BY 4.0 International license.

3. Discussion

To the best of our knowledge, our study investigated for the first time the effects of APOE4 genotypes, central obesity, and family history of dementia on the graph theoretical metrics of structural brain networks derived via tractography, in cognitively healthy adults. The advantage of our analysis methods over conventional structural network analyses lies in the use of integrated structural network matrices which combine, in a data-driven manner, multiple metrics of the white-matter tracts, rather than arbitrarily using one metric. This means that more information is included in the individual structural network matrices.

Graph theoretical metrics expressing segregation and integration of each participant's structural brain connectome were calculated for the whole-brain and for two sub-networks, the DMN (which is known to be impaired in AD) and the visual network (used here as a control network). Multivariate analyses revealed no significant effects for either whole-brain or for the sub-networks, which suggests that there are no differences in network measures for any of the risk factors (APOE4, family history of dementia or central obesity). This interesting finding, which indicates that the integration and segregation properties of these structural networks are preserved in individuals at heightened risk of developing AD, could point to a possible compensatory mechanism that leads to minimal functional disruption (as indicated by the normal cognitive abilities of our sample). We note, however, that it is not known when, or indeed if, any of these individuals would develop AD. Cortical-thickness based structural brain networks, which reflect different organisational properties to the tractography-derived networks used in our analysis, demonstrated altered properties in subjects with MCI and AD compared to healthy controls following the progress of the disease (Zhou & Liu, 2013). Additionally, Brown et al., 2011 found that tractography-derived structural brain networks in older APOE4 carriers exhibited loss of local interconnectivity in contrast to those of older non-carriers, and that the carriers had impaired memory abilities as well. Finally, Ma et al., 2017 found that structural brain connectivity was disrupted in adults (older than 55 years of age) as a result of an interaction between APOE4 status and developed MCI, more so than it was for APOE4 carriers only. These findings may suggest that structural connectivity changes are not

bioRxiv preprint doi: https://doi.org/10.1101/2020.10.08.331025; this version posted October 9, 2020. The copyright holder for this preprint (which was not certified by peer review) is the author/funder, who has granted bioRxiv a license to display the preprint in perpetuity. It is made available under aCC-BY 4.0 International license.

present in cognitively healthy individuals at risk, and reflect a manifestation of established disease and/or of older age.

Looking at the hubs of the whole-brain structural networks of low-risk versus high-risk individuals, we identified that the three subgroups of high-risk individuals (centrally obese, positive FH, and positive APOE4) when compared with individuals in the respective low-risk groups (normal weight, negative FH, and negative APOE4) consistently exhibited a hub in the right paracentral lobule. The paracentral lobule is located on the medial surface of the cerebral hemisphere and includes parts of both the frontal and parietal lobes. It has gyral projections to the medial frontal gyrus, cingulate sulcus, and precuneus and sulcal projections to the paracentral, cingulate, precentral sulci and the pars marginalis of cingulate sulcus. The paracentral lobule controls motor and sensory innervations of the contralateral lower limb. In a recent study, widespread cortical thinning in left hemisphere regions including pericalcarine cortex, supramarginal gyrus, cuneus cortex, lateral occipital cortex, precuneus cortex, fusiform gyrus, superior frontal gyrus, lateral occipital cortex, entorhinal cortex, inferior parietal cortex, isthmus-cingulate cortex, postcentral gyrus, superior parietal cortex, caudal middle frontal gyrus, insula cortex, precentral gyrus and paracentral lobule was observed in patients with AD compared to normal controls (Yang et al., 2019). Another structural MRI study on nondemented aging subjects revealed a modulation of the cortical thickness covariance between the left parahippocampal gyrus and left medial cortex, supplementary motor area, the left medial superior frontal gyrus, and paracentral lobule driven by the interaction of the rs405509 genotype and age (Chen et al., 2015). Rs405509 is an AD-related polymorphism located in the APOE promoter region that regulates the transcriptional activity of the APOE gene. Abnormal structural brain connectivity was identified between the angular gyrus, superior parietal gyrus, precuneus, posterior cingulum, putamen, precentral gyrus, postcentral gyrus, and paracentral lobule in elders with subjective cognitive decline compared to healthy controls (Kim et al., 2019). These aberrant structural connections were also associated with cognitive scores. If this novel phenotype can potentially predict the development of symptoms in a longitudinal study of the same cohort, it could be used as an early biomarker of dementia.

bioRxiv preprint doi: https://doi.org/10.1101/2020.10.08.331025; this version posted October 9, 2020. The copyright holder for this preprint (which was not certified by peer review) is the author/funder, who has granted bioRxiv a license to display the preprint in perpetuity. It is made available under aCC-BY 4.0 International license.

Assessment of our analysis

Our findings would benefit from replication in a larger sample due to the fragmentation of the initial sample into subgroups with the different risk profiles. It would also be beneficial for structural network analyses to include measures which are believed to play a more important role in the functional performance of the brain, such as myelination of the white matter tracts (Messaritaki et al., 2020) and axonal diameter. We finally note that the thresholding of structural connectivity matrices derived from tractography is still issue of debate. Buchanan et al., 2020; Civier et al., 2019; Drakesmith et al., 2015 have shown the possible effects of thresholding when different tractography methods are used. In our analysis, we adopted a modest thresholding of 5 streamlines, to reduce possible false positives.

4. Conclusion

In conclusion, our study did not detect any changes in structural brain networks that would imply alterations in the integration and segregation structural network properties in cognitively healthy individuals with different risk factors. We identified the right paracentral lobule as a hub brain area in high-risk individuals but not in low-risk individuals. A longitudinal study of the same cohort with the incorporation of functional neuroimaging data could evaluate this phenotype further.

Disclosures

The authors report no conflicts of interest.

Funding

- HC is funded by a Wellcome Trust Integrative Neuroscience PhD studentship [108891/B/15/Z]
- EM was partly funded by the BRAIN Biomedical Research Unit (which is funded by the Welsh Government through Health and Care Research Wales). EM is also funded by a Wellcome Trust ISSF3 Research Fellowship at Cardiff University [204824/Z/16/Z].

bioRxiv preprint doi: https://doi.org/10.1101/2020.10.08.331025; this version posted October 9, 2020. The copyright holder for this preprint (which was not certified by peer review) is the author/funder, who has granted bioRxiv a license to display the preprint in perpetuity. It is made available under aCC-BY 4.0 International license.

- SID was supported by MRC grant MR/K004360/1 (Behavioural and Neurophysiological Effects of Schizophrenia Risk Genes: A Multi-locus, Pathway Based Approach) and by a MARIE-CURIE COFUND EU-UK Research Fellowship.
- CMB was funded by a research fellowship from the Alzheimer's Society and the BRACE Alzheimer's Charity (grant ref: 208).

References

Badhwar, A. P., Tam, A., Dansereau, C., Orban, P., Hoffstaedter, F., & Bellec, P. (2017). Resting-state network dysfunction in Alzheimer's disease: A systematic review and meta-analysis. *Alzheimer's and Dementia: Diagnosis, Assessment and Disease Monitoring*, *8*, 73–85. https://doi.org/10.1016/j.dadm.2017.03.007

Basser, P. J., Pajevic, S., Pierpaoli, C., Duda, J., & Aldroubi, A. (2000). In vivo fiber tractography using DT-MRI data. *Magnetic Resonance in Medicine*, *44*(4), 625–632. https://doi.org/10.1002/1522-2594(200010)44:4<625::AID-MRM17>3.0.CO;2-O

Brown, J. A., Terashima, K. H., Burggren, A. C., Ercoli, L. M., Miller, K. J., Small, G. W., & Bookheimer, S. Y. (2011). Brain network local interconnectivity loss in aging APOE-4 allele carriers. *Proceedings of the National Academy of Sciences of the United States of America*, *108*(51), 20760–20765. https://doi.org/10.1073/pnas.1109038108

Buchanan, C. R., Bastin, M. E., Ritchie, S. J., Liewald, D. C., Madole, J. W., Tucker-Drob, E. M., Deary, I. J., & Cox, S. R. (2020). The effect of network thresholding and weighting on structural brain networks in the UK Biobank. *NeuroImage*, *211*(November 2019), 116443. https://doi.org/10.1016/j.neuroimage.2019.116443

Buckner, R. L., Sepulcre, J., Talukdar, T., Krienen, F. M., Liu, H., Hedden, T., Andrews-Hanna, J. R., Sperling, R. A., & Johnson, K. A. (2009). Cortical hubs revealed by intrinsic functional connectivity: Mapping, assessment of stability, and relation to Alzheimer's disease. *Journal of Neuroscience*, *29*(6), 1860–1873.

bioRxiv preprint doi: https://doi.org/10.1101/2020.10.08.331025; this version posted October 9, 2020. The copyright holder for this preprint (which was not certified by peer review) is the author/funder, who has granted bioRxiv a license to display the preprint in perpetuity. It is made available under aCC-BY 4.0 International license.

https://doi.org/10.1523/JNEUROSCI.5062-08.2009

Bullmore, E., & Sporns, O. (2009). Complex brain networks: Graph theoretical analysis of structural and functional systems. *Nature Reviews Neuroscience*, *10*(3), 186–198. https://doi.org/10.1038/nrn2575

Bullmore, E. T., & Bassett, D. S. (2011). Brain graphs: Graphical models of the human brain connectome. *Annual Review of Clinical Psychology*, *7*, 113–140. https://doi.org/10.1146/annurev-clinpsy-040510-143934

Chen, Y., Li, P., Gu, B., Liu, Z., Li, X., Evans, A. C., Gong, G., & Zhang, Z. (2015). The effects of an APOE promoter polymorphism on human cortical morphology during nondemented aging. *Journal of Neuroscience*, *35*(4), 1423–1431. https://doi.org/10.1523/JNEUROSCI.1946-14.2015

Civier, O., Smith, R. E., Yeh, C. H., Connelly, A., & Calamante, F. (2019). Is removal of weak connections necessary for graph-theoretical analysis of dense weighted structural connectomes from diffusion MRI? *NeuroImage*, *194*(November 2018), 68–81. https://doi.org/10.1016/j.neuroimage.2019.02.039

Coad, B. M., Craig, E., Louch, R., Aggleton, J. P., Vann, S. D., & Metzler-Baddeley, C. (2020). Precommissural and postcommissural fornix microstructure in healthy aging and cognition. *Brain and Neuroscience Advances*, *4*, 239821281989931. https://doi.org/10.1177/2398212819899316

Dai, Z., Lin, Q., Li, T., Wang, X., Yuan, H., Yu, X., He, Y., & Wang, H. (2019). Disrupted structural and functional brain networks in Alzheimer's disease. *Neurobiology of Aging*, *75*, 71–82. https://doi.org/10.1016/j.neurobiolaging.2018.11.005

Dell'Acqua, F., Scifo, P., Rizzo, G., Catani, M., Simmons, A., Scotti, G., & Fazio, F. (2010). A modified damped Richardson-Lucy algorithm to reduce isotropic background effects in spherical deconvolution. *NeuroImage*, *49*(2), 1446–1458.

bioRxiv preprint doi: https://doi.org/10.1101/2020.10.08.331025; this version posted October 9, 2020. The copyright holder for this preprint (which was not certified by peer review) is the author/funder, who has granted bioRxiv a license to display the preprint in perpetuity. It is made available under aCC-BY 4.0 International license.

https://doi.org/10.1016/j.neuroimage.2009.09.033

Dimitriadis, S. I., Antonakakis, M., Simos, P., Fletcher, J. M., & Papanicolaou, A. C. (2017). Data-Driven Topological Filtering Based on Orthogonal Minimal Spanning Trees: Application to Multigroup Magnetoencephalography Resting-State Connectivity. *Brain Connectivity*, *7*(10), 661–670. https://doi.org/10.1089/brain.2017.0512

Dimitriadis, S. I., Drakesmith, M., Bells, S., Parker, G. D., Linden, D. E., & Jones, D. K. (2017). Improving the Reliability of Network Metrics in Structural Brain Networks by Integrating Different Network Weighting Strategies into a Single graph. *Frontiers in Neuroscience*, *11*(December). https://doi.org/10.3389/fnins.2017.00694

Dimitriadis, S. I., Laskaris, N. A., Tsirka, V., Vourkas, M., Micheloyannis, S., & Fotopoulos, S. (2010). Tracking brain dynamics via time-dependent network analysis. *Journal of Neuroscience Methods*, *193*(1), 145–155. https://doi.org/10.1016/j.jneumeth.2010.08.027

Dimitriadis, S. I., Messaritaki, E., & Jones, D. K. (2020). The Impact of Graph Construction Scheme and Community Detection Algorithm on the Reliability of Community and Hub Identification in Structural Brain Networks. *BioRXiv*. https://doi.org/https://doi.org/10.1101/2020.05.07.082271

Drakesmith, M., Caeyenberghs, K., Dutt, A., Lewis, G., David, A. S., & Jones, D. K. (2015). Overcoming the effects of false positives and threshold bias in graph theoretical analyses of neuroimaging data. *NeuroImage*, *118*, 313–333. https://doi.org/10.1016/j.neuroimage.2015.05.011

Folstein, M. F., Folstein, S. E., & McHugh, P. R. (1975). “Mini-Mental state”. A practical methos for grading the cognitive state of patients for the clinician. *Journal of Psychiatric Research*, *12*, 189–198. https://doi.org/10.1016/0022-3956(75)90026-6

Hebert, L. E., Weuve, J., Scherr, P. A., & Evans, D. A. (2013). Alzheimer disease in the United

bioRxiv preprint doi: https://doi.org/10.1101/2020.10.08.331025; this version posted October 9, 2020. The copyright holder for this preprint (which was not certified by peer review) is the author/funder, who has granted bioRxiv a license to display the preprint in perpetuity. It is made available under aCC-BY 4.0 International license.

States (2010–2050) estimated using the 2010 census. *American Academy of Neurology*, *80*(19), 1778–1783. https://doi.org/10.1212/WNL.0b013e31828726f5

IBM Corp. (2019). *Released 2019. IBM SPSS Statistics for Macintosh, Version 26.0. Armonk, NY: IBM Corp.*

Irfanoglu, M. O., Walker, L., Sarlls, J., Marenco, S., & Pierpaoli, C. (2012). Effects of image distortions originating from susceptibility variations and concomitant fields on diffusion MRI tractography results. *NeuroImage*, *61*(1), 275–288. https://doi.org/10.1016/j.neuroimage.2012.02.054

John, M., Ikuta, T., & Ferbinteanu, J. (2017). Graph analysis of structural brain networks in Alzheimer's disease: beyond small world properties. *Brain Structure and Function*, *222*(2), 923–942. https://doi.org/10.1007/s00429-016-1255-4

Jones, D. K., Horsfield, M. A., & Simmons, A. (1999). Optimal strategies for measuring diffusion in anisotropic systems by magnetic resonance imaging. *Magnetic Resonance in Medicine*, *42*(3), 515–525. https://doi.org/10.1002/(SICI)1522-2594(199909)42:3<515::AID-MRM14>3.0.CO;2-Q

Kim, D., Lee, S., Choi, M., Youn, H. C., Suh, S., Jeong, H. G., & Han, C. E. (2019). Diffusion tensor imaging reveals abnormal brain networks in elderly subjects with subjective cognitive deficits. *Neurological Sciences*, *40*(11), 2333–2342. https://doi.org/10.1007/s10072-019-03981-6

Kroenke, K., Spitzer, R. L., & Williams, J. B. W. (2001). The PHQ-9: Validity of a Brief Depression Severity Measure. *Journal of General Internal Medicine*, *16*, 606–613. https://doi.org/10.1046/j.1525-1497.2001.016009606.x

Leemans, A., Jeurissen, B., Sijbers, J., & Jones, D. K. (2009). ExploreDTI: a graphical toolbox for processing, analyzing, and visualizing diffusion MR data. *17th Annual Meeting of the International Society for Magnetic Resonance in Medicine, Hawaii, USA*, 3537.

bioRxiv preprint doi: https://doi.org/10.1101/2020.10.08.331025; this version posted October 9, 2020. The copyright holder for this preprint (which was not certified by peer review) is the author/funder, who has granted bioRxiv a license to display the preprint in perpetuity. It is made available under aCC-BY 4.0 International license.

Livingston, G., Huntley, J., Sommerlad, A., Ames, D., Ballard, C., Banerjee, S., Brayne, C., Burns, A., Cohen-Mansfield, J., Cooper, C., Costafreda, S. G., Dias, A., Fox, N., Gitlin, L. N., Howard, R., Kales, H. C., Kivimäki, M., Larson, E. B., Ogunniyi, A., … Mukadam, N. (2020). Dementia prevention, intervention, and care: 2020 report of the Lancet Commission. *The Lancet*, *396*(10248), 413–446. https://doi.org/10.1016/S0140-6736(20)30367-6

Lo, C. Y., Wang, P. N., Chou, K. H., Wang, J., He, Y., & Lin, C. P. (2010). Diffusion tensor tractography reveals abnormal topological organization in structural cortical networks in Alzheimer's disease. *Journal of Neuroscience*, *30*(50), 16876–16885. https://doi.org/10.1523/JNEUROSCI.4136-10.2010

Ma, C., Wang, J., Zhang, J., Chen, K., Li, X., Shu, N., Chen, Y., Liu, Z., & Zhang, Z. (2017). Disrupted Brain Structural Connectivity: Pathological Interactions Between Genetic APOE ε4 Status and Developed MCI Condition. *Molecular Neurobiology*, *54*(9), 6999–7007. https://doi.org/10.1007/s12035-016-0224-5

Messaritaki, E., Dimitriadis, S. I., & Jones, D. K. (2019). Optimization of graph construction can significantly increase the power of structural brain network studies. *NeuroImage*, *199*(February), 495–511. https://doi.org/10.1016/j.neuroimage.2019.05.052

Messaritaki, E., Foley, S., Schiavi, S., Magazzini, L., Routley, B., Jones, D. K., & Singh, K. D. (2020). Predicting MEG resting-state functional connectivity using microstructural information. *BioRxiv*, 1–26. https://doi.org/10.1101/2020.09.15.298307

Metzler-baddeley, C., Mole, J. P., Leonaviciute, E., Sims, R., Kidd, E. J., Ertefai, B., Kelso-mitchell, A., Gidney, F., Fasano, F., Evans, J., Jones, D. K., & Baddeley, R. J. (2019). Sex-specific effects of central adiposity and inflammatory markers on limbic microstructure. *Neuroimage*, *189*, 793–803. https://doi.org/10.1016/j.neuroimage.2019.02.007

Metzler-baddeley, C., Mole, J. P., Sims, R., Fasano, F., Evans, J., Jones, D. K., Aggleton, J.

bioRxiv preprint doi: https://doi.org/10.1101/2020.10.08.331025; this version posted October 9, 2020. The copyright holder for this preprint (which was not certified by peer review) is the author/funder, who has granted bioRxiv a license to display the preprint in perpetuity. It is made available under aCC-BY 4.0 International license.

P., & Baddeley, R. J. (2019). Fornix white matter glia damage causes hippocampal gray matter damage during age-dependent limbic decline. *Scientific Reports*, *9*, 1060. https://doi.org/10.1038/s41598-018-37658-5

Mole, J. P., Fasano, F., Evans, J., Sims, R., Hamilton, D. A., Kidd, E., & Metzler-Baddeley, C. (2020). Genetic risk of dementia modifies obesity effects on white matter myelin in cognitively healthy adults. *Neurobiology of Aging*, *94*, 298–310. https://doi.org/10.1016/j.neurobiolaging.2020.06.014

Mukherjee, P., Berman, J. I., Chung, S. W., Hess, C. P., & Henry, R. G. (2008). Diffusion tensor MR imaging and fiber tractography: Theoretic underpinnings. *American Journal of Neuroradiology*, *29*(4), 632–641. https://doi.org/10.3174/ajnr.A1051

Mukherjee, P., Chung, S. W., Berman, J. I., Hess, C. P., & Henry, R. G. (2008). Diffusion tensor MR imaging and fiber tractography: Technical considerations. *American Journal of Neuroradiology*, *29*(5), 843–852. https://doi.org/10.3174/ajnr.A1052

Nelson, H. E. (1991). The National Adult Reading Test-Revised (NART-R): test manual. *National Foundation for Educational Research-Nelson, Windsor, UK*.

Neumann, J., Lohmann, G., Derrfuss, J., & Von Cramon, D. Y. (2005). Meta-analysis of functional imaging data using replicator dynamics. *Human Brain Mapping*, *25*(1), 165–173. https://doi.org/10.1002/hbm.20133

Parker, G. D. (2014). *Robust Processing of Diffusion Weighted Image Data. Unpublished PhD Thesis. Cardiff University*.

Power, J. D., Cohen, A. L., Nelson, S. M., Wig, G. S., Anne, K., Church, J. A., Vogel, A. C., Laumann, T. O., & Miezin, F. M. (2011). Functional network organization of the human brain. *Neuron*, *72*(4), 665–678. https://doi.org/10.1016/j.neuron.2011.09.006

Rubinov, M., & Sporns, O. (2010). Complex network measures of brain connectivity: Uses and interpretations. *NeuroImage*. https://doi.org/10.1016/j.neuroimage.2009.10.003

bioRxiv preprint doi: https://doi.org/10.1101/2020.10.08.331025; this version posted October 9, 2020. The copyright holder for this preprint (which was not certified by peer review) is the author/funder, who has granted bioRxiv a license to display the preprint in perpetuity. It is made available under aCC-BY 4.0 International license.

Tuch, D. S., Reese, T. G., Wiegell, M. R., Makris, N., Belliveau, J. W., & Van Wedeen, J. (2002). High angular resolution diffusion imaging reveals intravoxel white matter fiber heterogeneity. *Magnetic Resonance in Medicine*, *48*(4), 577–582. https://doi.org/10.1002/mrm.10268

Tzourio-Mazoyer, N., Landeau, B., Papathanassiou, D., Crivello, F., Etard, O., Delcroix, N., Mazoyer, B., & Joliot, M. (2002). Automated Anatomical Labeling of Activations in SPM Using a Macroscopic Anatomical Parcellation of the MNI MRI Single-Subject Brain. *NeuroImage*, *15*(1), 273–289. https://doi.org/10.1006/NIMG.2001.0978

van den Heuvel, M. P., & Sporns, O. (2013). Network hubs in the human brain. *Trends in Cognitive Sciences*, *17*(12), 683–696. https://doi.org/10.1016/j.tics.2013.09.012

Wang, L., Roe, C. M., Snyder, A. Z., Matthew, R., Thomas, J. B., Xiong, C., Benzinger, T. L., Morris, J. C., & Ances, B. M. (2012). Alzheimer's disease family history impacts resting state functional connectivity. *Ann Neurology*, *72*(4), 571–577. https://doi.org/10.1002/ana.23643

Yang, H., Xu, H., Li, Q., Jin, Y., Jiang, W., Wang, J., Wu, Y., Li, W., Yang, C., Li, X., Xiao, S., Shi, F., & Wang, T. (2019). Study of brain morphology change in Alzheimer's disease and amnestic mild cognitive impairment compared with normal controls. *General Psychiatry*, *32*(2), 1–9. https://doi.org/10.1136/gpsych-2018-100005

Zhou, Y., & Liu, Y. W. (2013). Small-World Properties in Mild Cognitive Impairment and Early Alzheimer's Disease: A Cortical Thickness MRI Study Yongxia. *ISRN Geriatrics*. https://doi.org/doi:10.1155/2013/542080

bioRxiv preprint doi: https://doi.org/10.1101/2020.10.08.331025; this version posted October 9, 2020. The copyright holder for this preprint (which was not certified by peer review) is the author/funder, who has granted bioRxiv a license to display the preprint in perpetuity. It is made available under aCC-BY 4.0 International license.

Tables

Table 1:

	Mean (σ)			
Age	55.76 (8.22), Range: 38-71			
Males	71/165			
Years of Education	16.55 (3.32), Range: 9.5-26			
FH of dementia	59/163			
APOE4 carriers	64/164			
Waist Hip Ratio – Obese	102/165			
Demographics broken down by risk factor				
	N (M)	**N (F)**	**Mean age, M (σ)**	**Mean age, F (σ)**
No FH, No APOE4, Healthy weight	4	16	53.75 (4.03)	53.69 (8.68)
FH, No APOE4, Heathy weight	0	13	-	53.85 (6.87)
No FH, APOE4, Healthy weight	3	16	49.00 (7.21)	52.88 (9.64)
No FH, No APOE4, Obese	18	21	56.17 (8.74)	56.05 (7.68)
FH, APOE4, Healthy weight	4	6	59.00 (2.45)	59.83 (5.19)
No FH, APOE4, Obese	20	6	54.00 (9.61)	58.67 (6.56)
FH, No APOE4, Obese	17	10	58.71 (7.71)	56.60 (9.35)
FH, APOE4, Obese	5	3	57.00 (8.22)	62.00 (7.94)

Table 1. Participant Demographics. This table lists the demographics (age, years of education, sex) of the participants that took part in this study, and splits male (M) and female (F) data by risk factor group. FH = family history of dementia, APOE4 = Apolipoprotein ε4, and waist-hip ratio. Mean age and years of education, accurate to 2 decimal places, are quoted with standard deviations reported in brackets (σ).

Table 2:

Name of dMRI metric	**Abbreviation**
Number of tracts	NS
Percentage of tracts,	PS
Average tract length	ATL
Euclidean distance	ED
Streamline density	SLD
Tract volume	TV
Mean diffusivity	MD
Radial diffusivity	RD
Axial diffusivity	AxD
Fractional anisotropy	FA

Table 2. Abbreviations used for the dMRI metrics. This table defines the abbreviations used throughout the manuscript for each of the diffusion-weighted magnetic resonance imaging (dMRI) metrics.

bioRxiv preprint doi: https://doi.org/10.1101/2020.10.08.331025; this version posted October 9, 2020. The copyright holder for this preprint (which was not certified by peer review) is the author/funder, who has granted bioRxiv a license to display the preprint in perpetuity. It is made available under aCC-BY 4.0 International license.

Table 3:

sValue	CondIdx	AxD	ATL	ED	FA	MD	NS	PS	RD	SLD	TV
2.7153	1	0	0.001	0.0013	0.0001	0	0.0004	0.0005	0	0.0029	0.001
1.3103	2.0722	0	0.0021	0.0047	0.0001	0	0.0074	0.0104	0	0	0.0082
0.7989	3.399	0	0.0073	0.0065	0	0	0.0002	0.0005	0	0.4447	0.0034
0.3047	8.91	0	0.0299	0.3087	0.0001	0	0.0155	0.1257	0	0.0001	0.3775
0.2837	9.5698	0	0.0521	0.3839	0.0063	0	0.0018	0.043	0	0.3094	0.1527
0.2258	12.0263	0	0.7593	0.1808	0	0	0.0041	0.1228	0	0.1427	0.1425
0.1587	17.1051	0	0.0497	0.0493	0.0007	0	0.969	0.693	0	0.0078	0.3067
0.1433	18.9544	0	0.085	0.0034	0.2084	0	0.0016	0.0037	0	0.0732	0.0074
0.0414	65.5353	0	0.0135	0.0614	0.7839	0	0	0.0003	0	0.0192	0.0005
0	2.26E+14	1	0	0.0001	0.0004	1	0	0	1	0	0

Table 3. Belsley collinearity diagnostics results for dMRI connectivity matrices. Belsley collinearity diagnostics run across the diffusion-weighted magnetic resonance imaging (dMRI) metrics demonstrated multicollinearity between AxD, MD and RD. sValue = Singular values, CondIdx = Condition Index. Abbreviations of the dMRI metrics are defined in Table 2.

Table 4:

	ATL	AxD	SLD	FA	ED	MD	NS	PS	RD	TV
ATL	1.0000	0.4033	-0.5558	0.4772	0.5727	0.1638	-0.2631	-0.2599	-0.1635	-0.0986
AD	0.4033	1.0000	-0.2418	0.6036	0.1300	0.7722	-0.0373	-0.0270	0.1630	0.0446
SLD	-0.5558	-0.2418	1.0000	-0.4588	-0.4509	0.0311	0.1426	0.1253	0.2989	0.0322
FA	0.4772	0.6036	-0.4588	1.0000	0.2474	-0.0300	0.0101	0.0262	-0.6721	0.0871
ED	0.5727	0.1300	-0.4509	0.2474	1.0000	-0.0089	-0.4070	-0.4122	-0.1485	-0.3529
MD	0.1638	0.7722	0.0311	-0.0300	-0.0089	1.0000	-0.0680	-0.0679	0.7527	-0.0146
NS	-0.2631	-0.0373	0.1426	0.0101	-0.4070	-0.0680	1.0000	0.9564	-0.0669	0.9021
PS	-0.2599	-0.0270	0.1253	0.0262	-0.4122	-0.0679	0.9564	1.0000	-0.0775	0.8600
RD	-0.1635	0.1630	0.2989	-0.6721	-0.1485	0.7527	-0.0669	-0.0775	1.0000	-0.0689
TV	-0.0986	0.0446	0.0322	0.0871	-0.3529	-0.0146	0.9021	0.8600	-0.0689	1.0000
After Excluding AxD, PS, RD and TV										
	ATL	**SLD**	**FA**	**ED**	**MD**	**NS**				
ATL	1									
SLD	-0.5558	1								
FA	0.4772	-0.4588	1							
ED	0.5727	-0.4509	0.2474	1						
MD	0.1638	0.0311	-0.0300	-0.0089	1					
NS	-0.2631	0.1426	0.0101	-0.4070	-0.0680	1				

Table 4. Correlation coefficients (R) as determined by MATLAB (corrcoef) between the individual connectivity metrics (abbreviations defined in table 2). The lower half of the table shows reduced inter-correlation coefficients after the analysis has been re-run with AxD, PS, RD and TV excluded

bioRxiv preprint doi: https://doi.org/10.1101/2020.10.08.331025; this version posted October 9, 2020. The copyright holder for this preprint (which was not certified by peer review) is the author/funder, who has granted bioRxiv a license to display the preprint in perpetuity. It is made available under aCC-BY 4.0 International license.

Table 5:

sValue	CondIdx	Diameter	Efficiency	Lambda	Radius	Clustering coefficient	Eccentricity
2.4172	1.0000	0.0001	0.0003	0.0001	0.0000	0.0004	0.0000
0.3748	6.4489	0.0006	0.0257	0.0038	0.0010	0.0374	0.0003
0.0890	27.1550	0.0440	0.3625	0.1359	0.0011	0.5189	0.0002
0.0812	29.7691	0.0640	0.5520	0.1607	0.0000	0.3796	0.0018
0.0395	61.2534	0.2325	0.0107	0.2996	0.7250	0.0146	0.0004
0.0205	118.0614	0.6589	0.0487	0.4000	0.2729	0.0492	0.9972

Table 5. Belsley collinearity diagnostics results - network measures. This table demonstrates multilinearity between whole-brain diameter and mean eccentricity when assessed with Belsley collinearity diagnostics. sValue = Singular values, CondIdx = Condition Index.

Table 6:

Before Data Cleaning				
	Standardised Residual	**Statistic**	**DF**	**p-value**
Whole	Diameter	0.078	161	0.019
	Global efficiency	0.114	161	0.000
	Characteristic path length	0.082	161	0.010
	Radius	0.083	161	0.008
	Clustering coefficient	0.115	161	0.000
DMN	Diameter	0.118	161	0.000
	Global efficiency	0.200	161	0.000
	Characteristic path length	0.158	161	0.000
	Radius	0.120	161	0.000
	Clustering coefficient	0.146	161	0.000
Visual	Diameter	0.128	161	0.000
	Global efficiency	0.128	161	0.000
	Characteristic path length	0.124	161	0.000
	Radius	0.135	161	0.000
	Clustering coefficient	0.086	161	0.006
After Data Cleaning				
	Standardised Residual	**Statistic**	**DF**	**p-value**
Whole	Logged diameter	0.067	160	0.080
	Squared global efficiency	0.091	160	0.003
	Logged characteristic path length	0.047	160	0.200
	Logged radius	0.053	160	0.200
	Squared clustering coefficient	0.083	160	0.009
DMN	Logged diameter	0.059	151	0.200
	Squared global efficiency	0.151	151	0.000
	Logged characteristic path length	0.084	151	0.010
	Logged Radius	0.060	151	0.200
	Clustering coefficient	0.123	151	0.000
Visual	Logged diameter	0.091	161	0.003
	Squared global efficiency	0.108	161	0.000
	Logged characteristic path length	0.082	161	0.009
	Logged radius	0.088	161	0.004
	Squared clustering coefficient	0.060	161	0.200

bioRxiv preprint doi: https://doi.org/10.1101/2020.10.08.331025; this version posted October 9, 2020. The copyright holder for this preprint (which was not certified by peer review) is the author/funder, who has granted bioRxiv a license to display the preprint in perpetuity. It is made available under aCC-BY 4.0 International license.

Table 6. Kolmogorov-Smirnov test results for the whole-brain, DMN and visual system. Lack of normality of standardized residuals assessed with Kolmogorov-Smirnov tests of the whole-brain, DMN (default mode network) and visual system. The lower part of the table demonstrates how the normality of the metrics are improved after data cleaning (removing outliers and transforming the data). DF = degrees of freedom.

Table 7:

Whole-brain analysis			
Effect	**F**	**DF**	**p-value**
Intercept	48.648	5, 145	0.000
Sex	0.841	5, 145	0.523
Age	1.325	5, 145	0.257
Years of Education	1.904	5, 145	0.097
FH	1.307	5, 145	0.264
APOE4	0.351	5, 145	0.881
WHR	0.981	5, 145	0.432
FH X APOE4	1.019	5, 145	0.409
FH X WHR	0.532	5, 145	0.752
APOE4 X WHR	0.533	5, 145	0.751
FH X APOE4 X WHR	1.666	5, 145	0.147
Default mode network analysis			
Intercept	84.361	5,136	0.000
Sex	1.315	5,136	0.261
Age	1.867	5,136	0.104
Years of Education	1.010	5,136	0.414
FH	1.523	5,136	0.187
APOE4	0.924	5,136	0.567
WHR	0.201	5,136	0.961
FH X APOE4	0.242	5,136	0.242
FH X WHR	0.733	5,136	0.733
APOE4 X WHR	0.940	5,136	0.940
FH X APOE4 X WHR	0.444	5,136	0.444
Visual system analysis			
Intercept	73.555	5,146	0.000
Sex	0.534	5,146	0.750
Age	1.989	5,146	0.084
Years of Education	1.314	5,146	0.261
FH	0.351	5,146	0.881
APOE4	0.901	5,146	0.482
WHR	1.179	5,146	0.322
FH X APOE4	0.284	5,146	0.921
FH X WHR	0.986	5,146	0.429
APOE4 X WHR	1.365	5,146	0.241
FH X APOE4 X WHR	2.089	5,146	0.070

Table 7. Multivariate results. There were no significant differences in network measures as a function of risk factors: family history of dementia (FH), Apolipoprotein ε4 genotype (APOE4) and waist-hip ratio (WHR) across the whole-brain, default mode network or a control sub-network (visual system). F = F statistic, DF = degrees of freedom.

bioRxiv preprint doi: https://doi.org/10.1101/2020.10.08.331025; this version posted October 9, 2020. The copyright holder for this preprint (which was not certified by peer review) is the author/funder, who has granted bioRxiv a license to display the preprint in perpetuity. It is made available under aCC-BY 4.0 International license.

Table 8:

Risk factor change	Hubs which remain the same	Hubs which are lost	Hubs which are gained
Negative FH → Positive FH	Right rolandic operculum Right Heschl's gyrus	Left rolandic operculum Right inferior parietal gyrus Left angular gyrus	Left inferior frontal gyrus opercular part Left paracentral lobule Right paracentral lobule
APOE4 non-carrier → APOE4 carrier	Right rolandic operculum Right Heschl's gyrus	Left inferior frontal gyrus opercular part Right Precuneus	Right inferior parietal gyrus Left angular gyrus Right paracentral lobule
WHR healthy → WHR obese	Right rolandic operculum Right Heschl's gyrus	Left inferior frontal gyrus opercular part Right inferior parietal gyrus	Right paracentral lobule Left Heschl's gyrus

Table 8. Hub changes as a function of risk factor. The right rolandic operculum and right Heschl's gyrus remain constant when switching from a low-risk - no family history of dementia (FH), no Apolipoprotein ε4 (APOE4) allele, healthy waist-hip ratio (WHR) score - to a high-risk group (FH, APOE4 or obese). Whereas, the right paracentral lobule is consistently gained. Furthermore, a few more hubs are gained or lost, albeit inconsistent across risk factor groups.

bioRxiv preprint doi: https://doi.org/10.1101/2020.10.08.331025; this version posted October 9, 2020. The copyright holder for this preprint (which was not certified by peer review) is the author/funder, who has granted bioRxiv a license to display the preprint in perpetuity. It is made available under aCC-BY 4.0 International license.

Figures

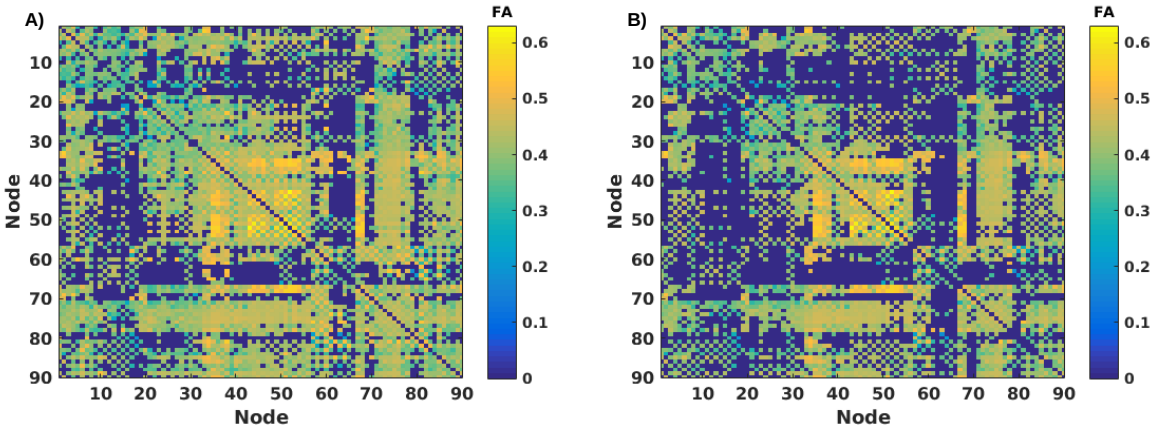

Figure 1. An example of the conservative threshold added to all dMRI connectivity matrices. A) Fractional anisotropy (FA) connectivity matrix for one participant before thresholding. **B)** After a conservative threshold of 5 streamlines was applied to FA for the same participant.

bioRxiv preprint doi: https://doi.org/10.1101/2020.10.08.331025; this version posted October 9, 2020. The copyright holder for this preprint (which was not certified by peer review) is the author/funder, who has granted bioRxiv a license to display the preprint in perpetuity. It is made available under aCC-BY 4.0 International license.

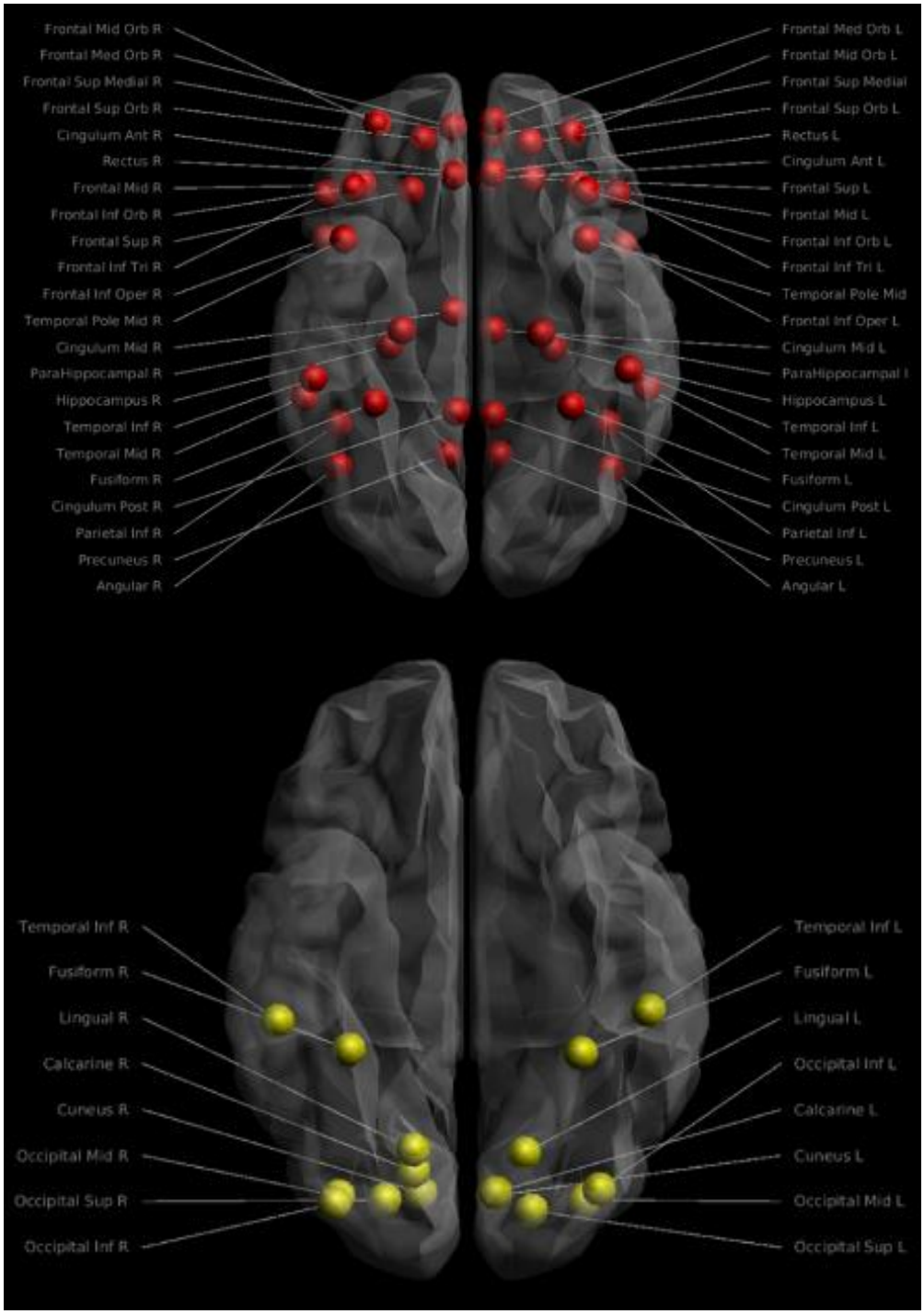

Figure 2. Nodes included in the subnetwork analysis for the default mode network (DMN) and visual system. The top figure shows the 44 nodes included in the DMN adapted from Power et al., 2011 whereas the bottom picture shows the 16 nodes included in the visual network adapted from Power et al., 2011. Images were created using ExploreDTI v4.8.6.

bioRxiv preprint doi: https://doi.org/10.1101/2020.10.08.331025; this version posted October 9, 2020. The copyright holder for this preprint (which was not certified by peer review) is the author/funder, who has granted bioRxiv a license to display the preprint in perpetuity. It is made available under aCC-BY 4.0 International license.

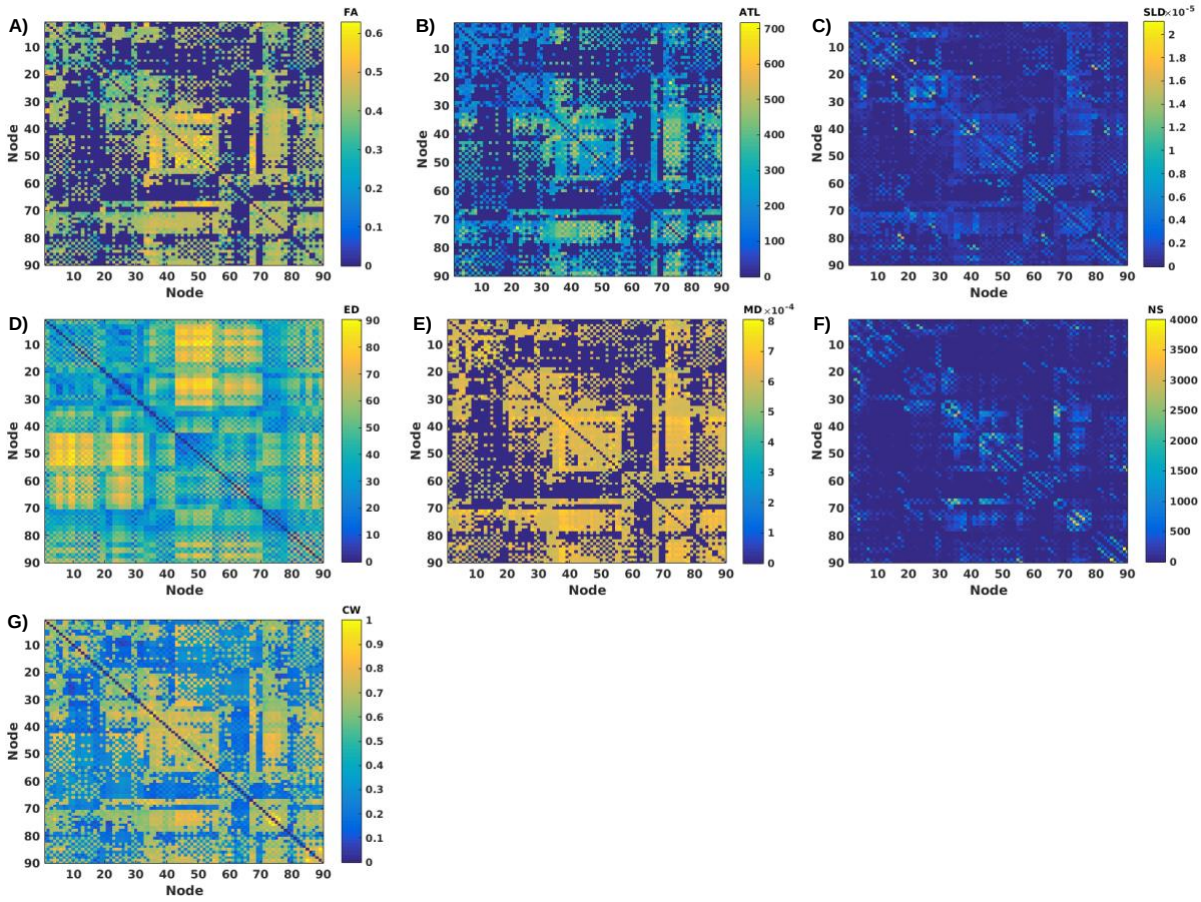

Figure 3. An example of the six Individual network measures that were combined into an integrated weighted structural brain network for one participant. A) FA, fractional anisotropy, **B)** ATL, average tract length **C)** SLD, streamline density, **D)** ED, Euclidean distance**, E)** MD**,** mean diffusivity **F)** NS, number of streamlines were combined into a **G)** integrated weighted structural brain network. CW = connectivity weight.

bioRxiv preprint doi: https://doi.org/10.1101/2020.10.08.331025; this version posted October 9, 2020. The copyright holder for this preprint (which was not certified by peer review) is the author/funder, who has granted bioRxiv a license to display the preprint in perpetuity. It is made available under aCC-BY 4.0 International license.

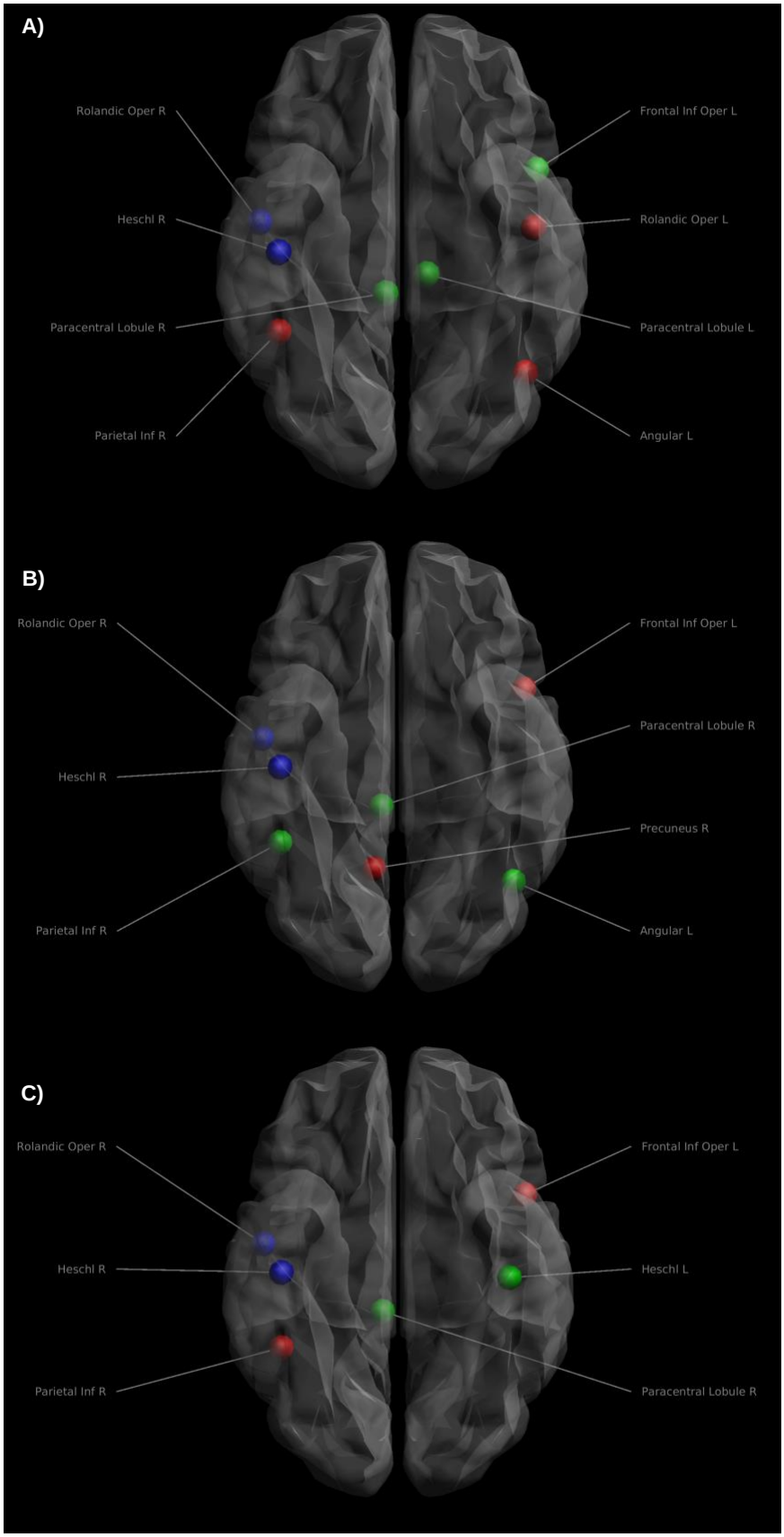

bioRxiv preprint doi: https://doi.org/10.1101/2020.10.08.331025; this version posted October 9, 2020. The copyright holder for this preprint (which was not certified by peer review) is the author/funder, who has granted bioRxiv a license to display the preprint in perpetuity. It is made available under aCC-BY 4.0 International license.

Figure 4. Nodes identified as hubs change dependent on risk factor profile. This figure shows the changes in nodes defined as hub regions, when you transition from a low-risk group to a high-risk group. **A)** Comparing individuals without a family history of dementia (FH) to those with a positive FH indicates that 2 hubs remain unchanged (blue), whereas 3 are gained (green) and 3 are lost (red). **B)** Comparing APOE4 non-carriers to carriers results in a gain of 3 hubs (green), loss of 2 hubs (red) but leaves 2 hubs unchanged (blue). **C)** In comparison to healthy individuals, obese participants gained 2 hubs (green), lost 2 hubs (red) and 2 hubs remains (blue).